Open access • Journal Article • DOI:10.1021/JP810852C

Imaging Gold Nanorods by Plasmon-Resonance-Enhanced Four Wave Mixing

Yookyung Jung, Hongtao Chen, Ling Tong, Ji-Xin Cheng

Institutions: Purdue University

Published on: 21 Jan 2009 - Journal of Physical Chemistry C (American Chemical Society)

Topics: Four-wave mixing and Surface plasmon resonance

2-1-2009

Imaging Gold Nanorods by Plasmon-Resonance-Enhanced Four Wave Mixing

Yookyung Jung
Purdue University - Main Campus, jung25@purdue.edu

Hongtao Chen
Purdue University - Main Campus, htchen@purdue.edu

Ling Tong
Purdue University - Main Campus, lingt@purdue.edu

Ji-Xin Cheng
Purdue University - Main Campus, jcheng@purdue.edu

THE JOURNAL OF PHYSICAL CHEMISTRY C LETTERS

2009, *113,* 2657–2663
Published on Web 01/21/2009

Imaging Gold Nanorods by Plasmon-Resonance-Enhanced Four Wave Mixing

Yookyung Jung,[†] Hongtao Chen,[‡] Ling Tong,[‡] and Ji-Xin Cheng[‡,§,*]

Department of Physics, Department of Chemistry, and Weldon School of Biomedical Engineering, Purdue University, West Lafayette, Indiana 47907

Received: December 9, 2008; Revised Manuscript Received: January 9, 2009

The current work investigates the four-wave mixing (FWM) signal from gold nanorods (NRs) using two synchronized lasers and its potential applications in bioimaging. Using the lightning rod model, we show that the strongest FWM occurs when the pump laser wavelength is tuned to be resonant with the longitudinal plasmon resonance wavelength of NR. The calculation is experimentally demonstrated by comparing the intensities of FWM from NRs with different plasmon resonance wavelengths. The FWM signal is further found to be enhanced by aggregation of NRs and is strongly dependent on pulse width. The FWM intensity from NRs is ~39 times stronger than the coherent anti-Stokes Raman scattering intensity from melamine beads. This plasmon-resonance-enhanced FWM signal enables NRs to be used as a nonlinear optical (NLO) imaging probe.

Gold nanostructures have been used as optical imaging agents in many ways. In the linear regime, plasmon scattering and absorption have been utilized for dark field microscopy[1,2] and photoacoustic tomography.[3−5] In the nonlinear regime, multiphoton luminescence has been recently observed from gold nanospheres,[6,7] nanorods,[8] nanoshells,[9] and nanowires.[10,11] Despite the brightness of the multiphoton luminescence, its spectral profile is generally broad and may overlap with fluorescence from other molecules in bioimaging study, which makes it hard to distinguish gold particles from other fluorescent molecules. On the other hand, four-wave mixing (FWM) signals from nanoparticles have narrow spectral profiles at well defined frequencies. FWM from coupled gold nanoparticles,[12] third harmonic generation (THG) from gold nanoparticles,[13,14] and coherent anti-Stokes scattering (CAS) from gold nanowires[10] have been recently reported. In order to apply these third order nonlinear optical processes to bioimaging, it is critical to generate a strong signal. However, previous studies did not show a strong FWM signal compared with multiphoton luminescence.[10,13,14] Although a large FWM signal was observed from coupled gold nanoparticles,[12] it is difficult to control the distance between two nanoparticles in biological applications.

A uniqueness of NRs lies in that their longitudinal plasmon resonance peak is tunable in the near-infrared (NIR) region by controlling the aspect ratio through synthesis.[15−17] Meanwhile, it has been known that gold nanoparticles have a large third order susceptibility when excited at the plasma resonance.[18,19] In this sense, NR provides an excellent candidate as a nonlinear optical imaging agent. So far, FWM from NRs has not been well investigated. Herein we show theoretical calculation and experimental demonstration of plasmon-resonance-enhanced FWM from NRs on a coverslip and inside live cells. The strong FWM signal renders NRs a competitive nonlinear optical imaging probe.

We carried out the FWM study on a laser-scanning coherent anti-Stokes Raman scattering (CARS) microscope that involves pump and Stokes excitation fields and a signal at the anti-Stokes wavelength. Because gold does not have any Raman active bands (Figure 1a), the FWM signal cannot be enhanced by vibrational resonance. Instead, gold NRs show transverse and longitudinal plasmon resonance. An enhanced two photon luminescence (TPL) from NR was shown by tuning the excitation wavelength to match the longitudinal plasmon resonance.[8] Likewise, we anticipate that the FWM signal can be enhanced when the pump, Stokes or the generated anti-Stokes field matches the plasmon resonance frequency as shown in Figure 1b.

We first explored the optimal condition of producing the strongest FWM signal using a lightning rod model.[20−22] To simplify the analysis, we assume that NR has a prolate spheroid shape with two equal minor axes, and the incident beam has linear polarization in parallel with the major axis. Then the relation between the incident field, E_{out}, and the field inside the gold spheroid, E_{in}, is given by[22]

$$E_{in} = \frac{\varepsilon_2}{\varepsilon_2 + A(\varepsilon_1 - \varepsilon_2)} E_{out} = L(\lambda, R) E_{out} \quad (1)$$

where ε_1 and ε_2 are dielectric constants of NR and surrounding medium. A is a shape dependent factor given by

$$A = \frac{ab^2}{2} \int_0^\infty \frac{ds}{(s+a^2)\sqrt{(s+a^2)(s+b^2)^2}} = \frac{1}{2R^2} \int_0^\infty \frac{dx}{(x+1)^{3/2}(x+1/R^2)} \quad (2)$$

where a is the semimajor axis and b is the semiminor axis, $R = a/b$ is the aspect ratio, and L is the local field factor. Because

* To whom correspondence should be addressed. E-mail: jcheng@purdue.edu.
† Department of Physics,
‡ Department of Chemistry,
§ Weldon School of Biomedical Engineering.

10.1021/jp810852c CCC: $40.75

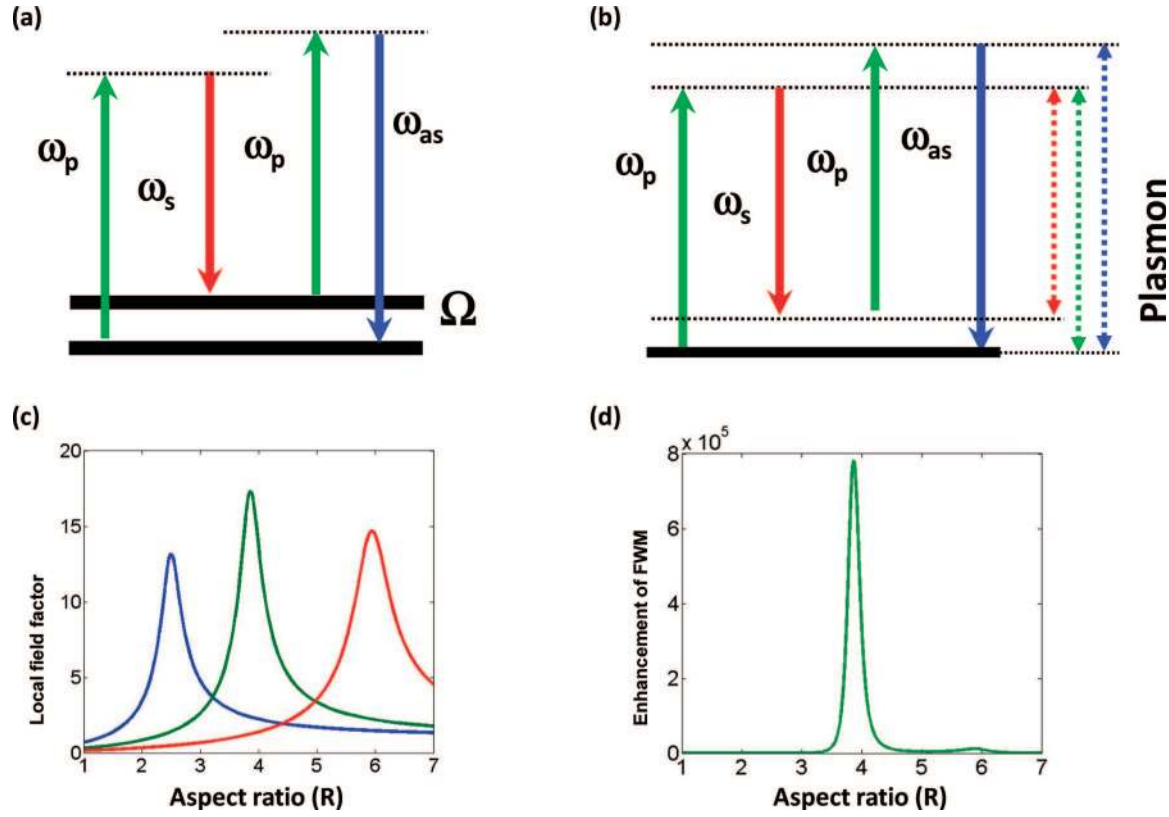

Figure 1. Enhancement of CARS and FWM generated by two incident beams at pump (ω_p) and Stokes (ω_s) wavelengths. (a) Energy diagram of vibrationally resonant CARS. (b) Energy diagram of FWM from NRs. When the plasmon resonance wavelength matches the pump, Stokes, or anti-Stokes wavelength, FWM is expected to be enhanced. (c) Relation between the aspect ratio of NR and the local field factor at each wavelength (blue: anti-Stokes; green: pump; red: Stokes) (d) Relation between aspect ratio of NR and FWM enhancement.

A is dependent on R and ε_1 is dependent on wavelength, the local field factor L is a function of both aspect ratio R and wavelength λ of the incident beam as shown by El-Sayed and co-workers.[15]

In our calculation, 790, 1018, and 645 nm are chosen as the pump, Stokes, and generated anti-Stokes wavelengths that will be used in the experiment. The effective relative dielectric constant of surrounding medium, cetyltrimethylammonium bromide (CTAB) is assumed to be 2.0.[23] The dependence of L on R is shown in Figure 1c. For the anti-Stokes, pump, and Stokes wavelengths, the local field factor (L) is maximized at the aspect ratio (R) of 2.5, 3.9, and 5.9, respectively. The induced polarization of NR at the anti-Stokes wavelength is given by

$$P_{\lambda_{as}}(R) = L_{\lambda_{as}}(R)\chi^{(3)}_{\lambda_{as}} L_{\lambda_p}(R)^2 L_{\lambda_s}(R)^* E_{\lambda_p}{}^2 E^*_{\lambda_s} \quad (3)$$

where $\chi^{(3)}$ is the third order susceptibility, and L_λ is the local field factor at each wavelength. The intensity of the FWM field is proportional to $P_{\lambda_{as}}$

$$I_{FWM}(R) \propto |\chi^{(3)}_{\lambda_{as}}|^2 |L_{\lambda_{as}}(R)|^2 |L_{\lambda_p}(R)|^4 |L_{\lambda_s}(R)|^2 |E_{\lambda_p}|^4 |E_{\lambda_s}|^2 \quad (4)$$

Based on the above equations, the relation between the enhancement factor $|L_{\lambda_{as}}(R)|^2|L_{\lambda_p}(R)|^4|L_{\lambda_s}(R)|^2$ and the aspect ratio, R, is calculated and shown in Figure 1d. A sharp peak of I_{FWM} appears at $R = 3.9$. Because this aspect ratio corresponds to the plasmon wavelength of 790 nm, we show that the FWM signal can be maximized when the pump beam is resonant with the longitudinal plasmon mode of the NR.

Details of our multimodal nonlinear optical microscope can be found elsewhere.[24] Briefly, a femtosecond (fs) laser (Mai Tai, Spectra-Physics, Fremont, CA) generated a 130-fs pulse at a wavelength of 790 nm and repetition rate of 80 MHz. 80% of the Mai Tai output was used to pump an optical parametric oscillator (OPO; Spectra-Physics, Fremont, CA) generating a signal beam at 1290 nm and an idler beam at 2036 nm. The frequency of the idler beam was doubled to 1018 nm by a PPLN crystal. This 1018 nm beam was used as the Stokes beam. The other 20% of the Mai Tai beam was used as the pump beam, which was collinearly combined with the Stokes beam after passing through a delay line. The combined beams were sent into a FV1000 laser-scanning microscope (Olympus America Inc., PA) and focused into a sample using a 60X/IR water objective lens with a numerical aperture of 1.2. The backward FWM signal was separated from the excitation laser by a dichroic mirror and detected by an external photomultiplier tube after passing through a 650/45 nm filter. The backward signal could also be delivered to internal spectral detectors which enable spectral analysis. CTAB coated NRs were prepared by seeded growth method.[25] The CTAB coating prevents aggregation of NRs in the solution.

The NR solution was sonicated for 1 min and dried on a coverslip at room temperature to form a NR-condensed ring of 3 mm diameter. The area inside the ring was used for imaging. A typical FWM image of NRs with a plasmon resonance wavelength of 788 nm is shown in Figure 2a. When the 790 nm pump beam and 1018 nm Stokes beam were desynchronized, the NRs were visualized with a TPL signal that was weaker than the FWM signal (Figure 2b). The existence of FWM and TPL were confirmed by spectral analysis of a single spot, as shown in Figure 2c. The TPL (black curve) shows a broad profile from 400 to 650 nm, whereas the FWM signal (red curve) exhibits a sharp peak centered at 645 nm with a FWHM of 15 nm. The TPL was generated by a 790 nm pump which was

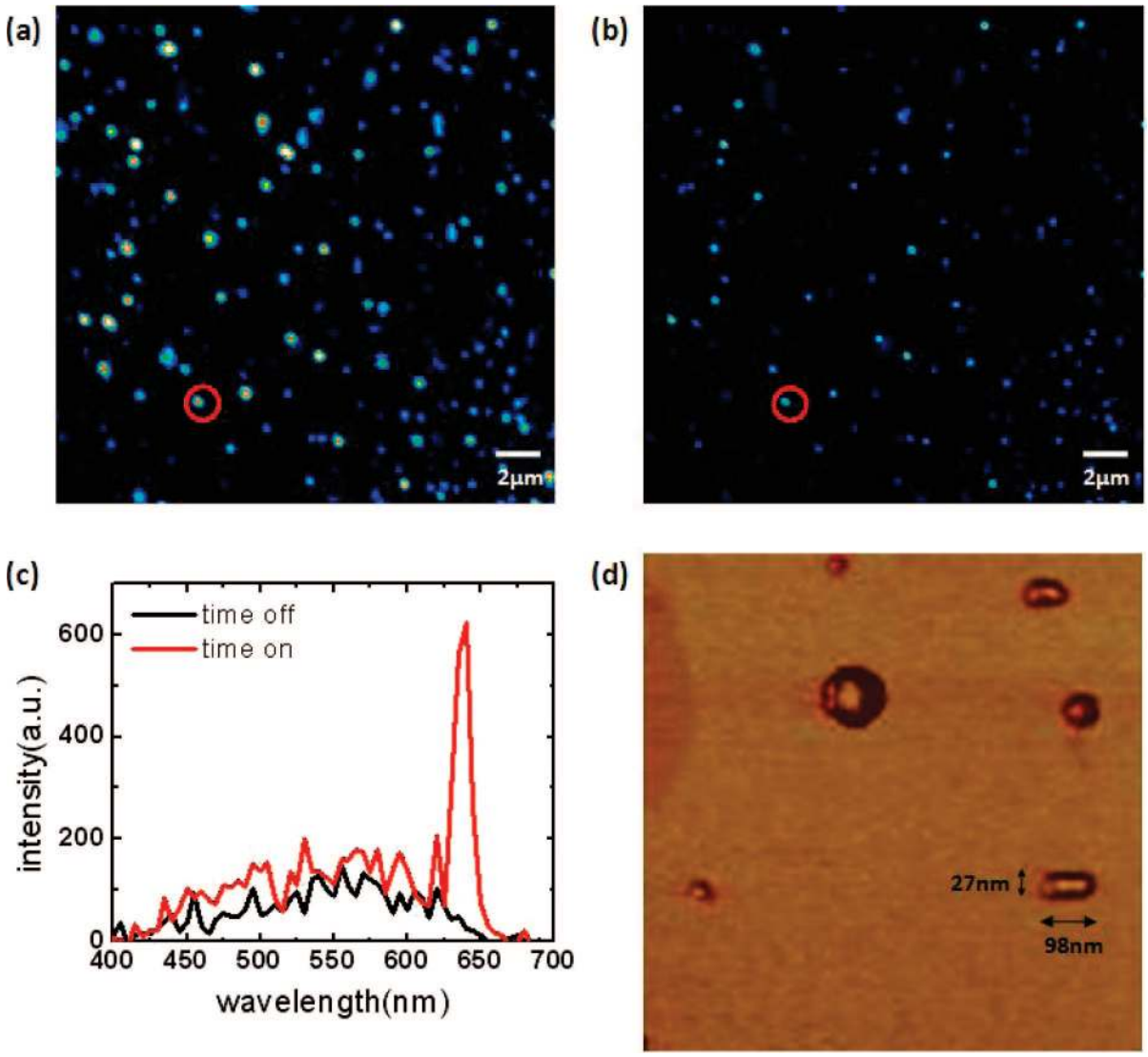

Figure 2. Imaging nanorods with FWM signal. (a and b) Images of NRs taken with the pump beam at 790 nm and the Stokes beams at 1018 nm synchronized and desynchronized. The values of the pump and Stokes beam power at the sample were 0.4 and 1.3 mW, respectively. (c) Emission spectrum of the circled spot. (d) AFM image of the same sample. Single NR, aggregates of NRs, and spherical nanoparticles were observed.

near the NR's longitudinal plasmon resonance. Notably, the FWM signal could be reproduced after resynchronizing the two lasers, indicating that NRs were photostable under the excitation with 21 pJ pulse energy.[26] To interrogate the status of NRs deposited on the coverslip, we acquired AFM images of the same sample. As shown in Figure 2d, individual nanorods with an aspect ratio around 3.6 coexist with aggregates of nanorods. The ratio of 3.6 is close to the calculated value of 3.9 that maximizes the FWM signal.

To inspect the relation between the aspect ratio R and the FWM signal strength, we acquired FWM images from NRs with 3 different aspect ratios, marked as NR661, NR788, and NR840. Here, the number after NR represents the plasmon resonance wavelength in nanometer, corresponding to the aspect ratio of 2.5, 3.9, and 5.9, respectively. All the samples were prepared from NR solutions at the same concentration of optical density = 15. Figure 3a−c shows the images of NR661, NR788, and NR840, respectively, with synchronized pump and Stokes beams. Because the signals contain contributions from both FWM and TPL, we further acquired TPL images of the same sample with two beams desynchronized. The difference between Figure 3 panels a−c and d−f, represents the FWM signal which has been confirmed by spectral analysis as shown in Figure 2c.

One difficulty in analyzing the FWM signal is that we cannot determine whether the signal comes from a single nanorod or an aggregate because of the diffraction limit of optical detection. Additionally, orientation of nanorods also affects the signal level because the FWM signal is dependent on the polarization of the incident beams.[10] To compare the FWM signal levels for NRs with different plasmon resonance wavelengths, we performed a statistical analysis by constructing histograms of the FWM intensity from each spot. The FWM signal was acquired by subtracting the TPL images from the TPL + FWM images of the same sample. The FWM intensity histograms from NR661, NR788, and NR840 are shown in Figure 3g−i. It was observed that, for NR788, most spots had an intensity level between 400 and 1600, whereas for NR661 and 840, the intensity level was below 400 for the majority of the spots examined. Figure 3j compares the average FWM intensity from NRs with different plasmon wavelengths. As expected, NR788 generates the strongest FWM signal. The average FWM intensity of NR788 is 9.2 times stronger than that of NR661 and 6.2 times stronger than that of NR840. The enhancement is not as great as expected by the calculation shown in Figure 1d. This discrepancy is attributed to the aggregations of NRs as discussed below.

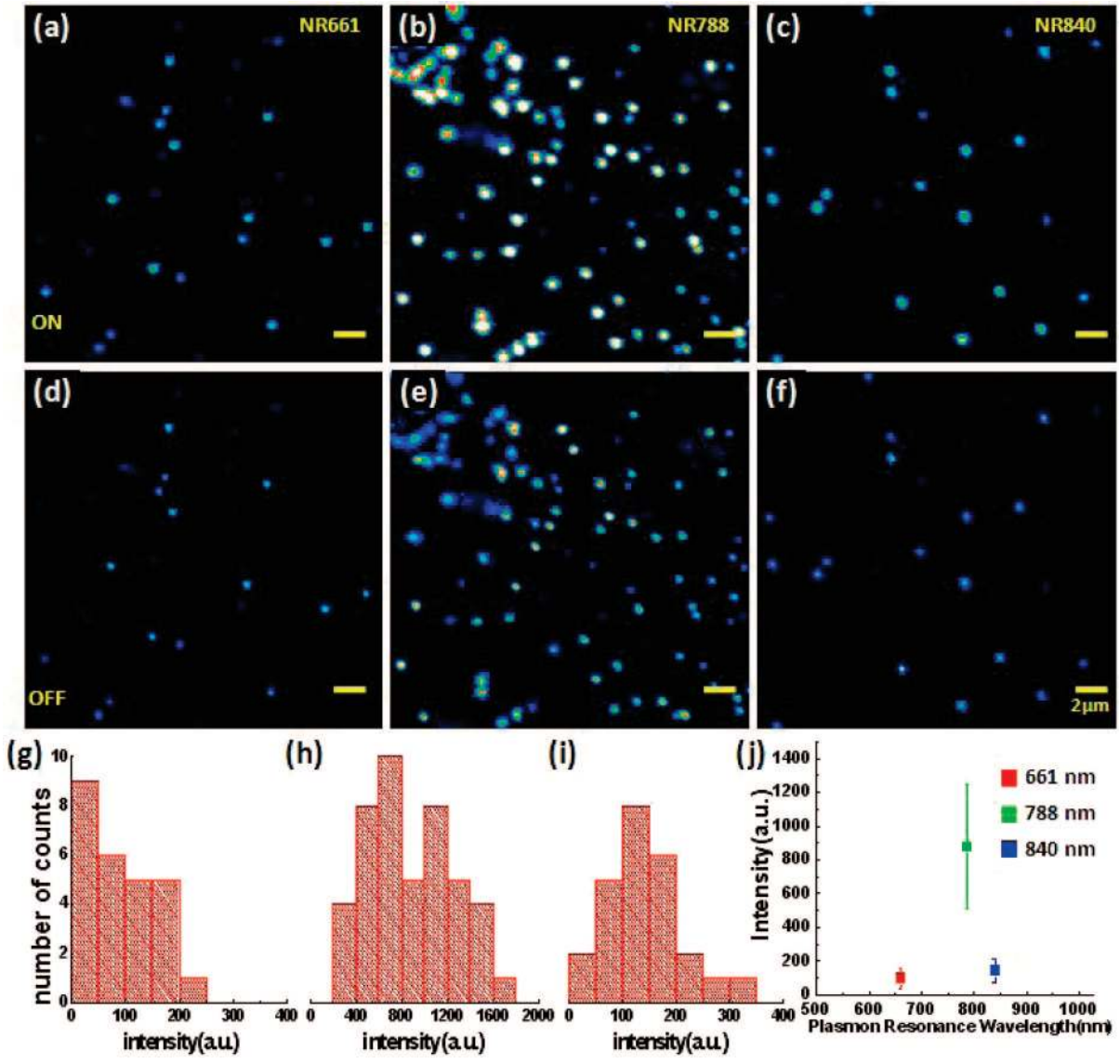

Figure 3. Dependence of FWM intensity on plasmon resonance wavelength. (a−c) Images of nanorods with plasmon resonance at 661 (a), 788 (b), and 840 nm (c). The pump and Stokes beams were synchronized, with average power values of 0.4 and 1.3 mW at the sample. (d−f) Images of the same samples with the same pump and Stokes beams but desynchronized. Bar length is 2 μm. (g−i) Intensity distributions of FWM for NR661, NR788, and NR840. (j) Average intensities of FWM from NRs with different plasmon resonance wavelengths.

We further observed that FWM could be enhanced not only by the surface plasmon resonance but also by the aggregation of NRs on the coverslip. Figure 4 compares the FWM intensity from a single and an aggregate of NR788. For these NRs, the surface plasmon resonance matches the pump laser wavelength. The TPL and FWM images were taken by desynchronizing and synchronizing the pump and Stokes beams. Panels a and b in Figure 4 show TPL and FWM images of a diffraction-limited spot, with intensity profiles shown in Figure 4c. The signal is attributed to a single nanorod based on the strong dependence on excitation polarization. The same analysis for an aggregate of NRs is shown in Figure 4d−f. It is interesting that the aggregate generated a much stronger FWM than a single NR. One may take it for granted that more particles generate a stronger signal. However, when we compared the TPL images of the single NR with the aggregate, we observed not so much difference. It is possible that the stronger FWM is due to the enhancement of *E*-field in the close gap between aggregated NRs.[12] According to the fractal aggregate theory,[27] the aggregate has a broad plasmon profile, which also explains the smaller difference in FWM intensities from three different NRs than calculated.

All of the above experiments were done using fs pulses at a pulse energy on the order of 10 pJ. Because picosecond pulses were widely used in CARS microscopy[28] and also CAS from gold nanowires,[10] we further investigated the optical response of NRs by ps laser excitation using a CARS microscope described elsewhere.[29] Briefly, the pump and Stokes laser beams were generated by two 5-ps Ti:sapphire lasers (Tsunami, Spectra-Physics) at wavelengths of 740 and 830 nm. The FWM signal at the anti-Stokes frequency, if generated, should be located at 668 nm. To check the existence of FWM from NR, we repetitively synchronized and desynchronized the two beams, and the images of NR are taken in the same way as the previous experiments. 650/45 filter was used to detect the signal. Figure 5a−c shows images with the pump and Stokes beams synchronized, desynchronized, and resynchronized. Figure 5d shows the average intensity of the circled area in Figure 5a−c

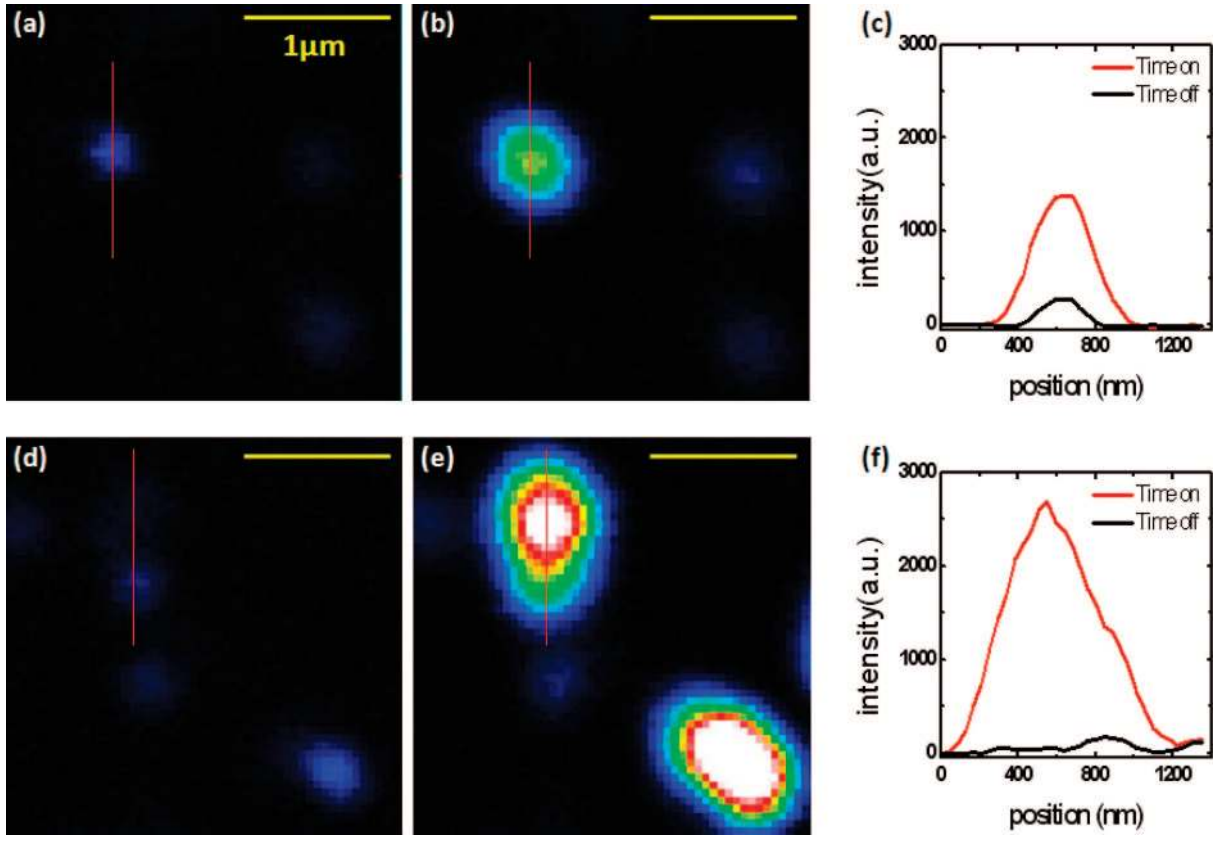

Figure 4. Comparison of FWM from a single NR and from closely located NRs. (a) Image of single NRs with pump and Stokes beams desynchronized. (b) Image of single NRs with pump and Stokes beams synchronized. (c) Intensity profile along the red line in (a and b). (d) Image of closely located NRs with pump and Stokes beams desynchronized. (e) Image of closely located NRs with pump and Stokes beams synchronized. (f) Intensity profile along the red lines in (d and e). Bar length is 1 μm.

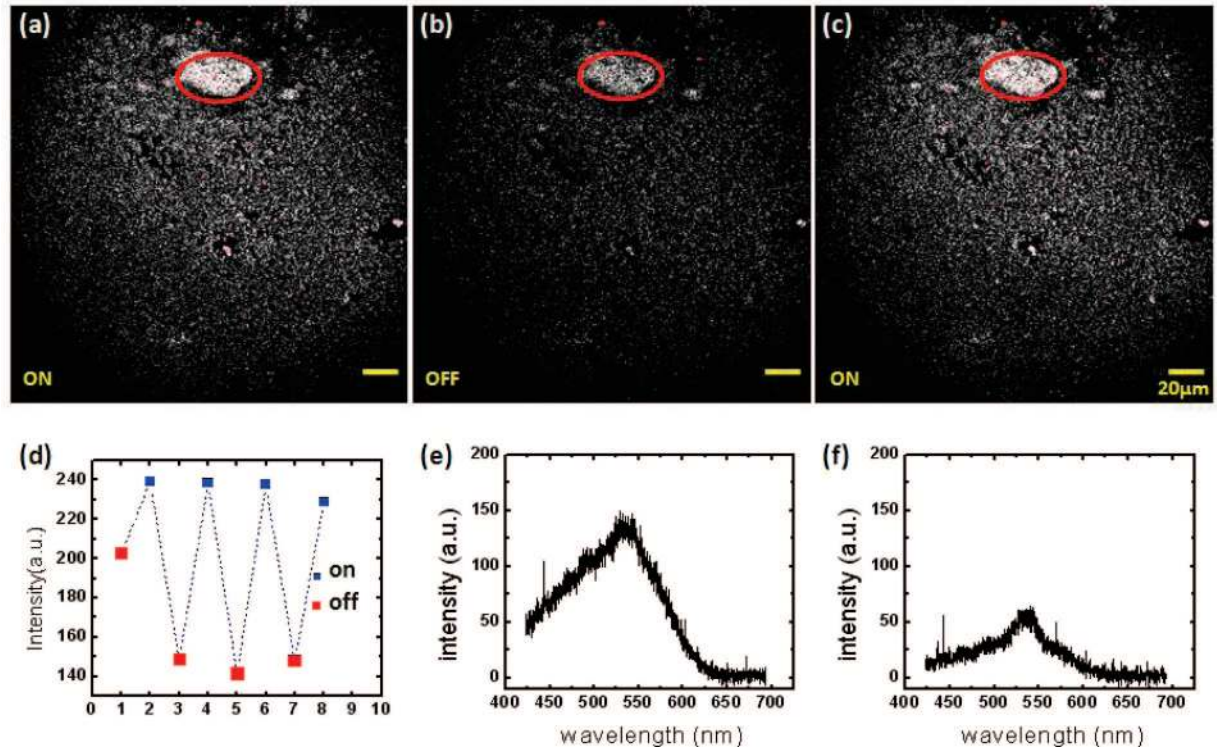

Figure 5. Nonlinear optical response from NR using 5-ps laser excitation. (a) TPL image of NRs with pump and Stokes beams synchronized. (b) TPL image of the same sample with pump and Stokes beams desynchronized. (c) TPL image of the same sample with pump and Stokes beams resynchronized. Bar length is 20 μm. (d) Average intensity of the circled area according to repetitive synchronization and desynchronization. (e and f) Emission spectrum of the circled area with pump and Stokes beams synchronized and desynchronized, respectively.

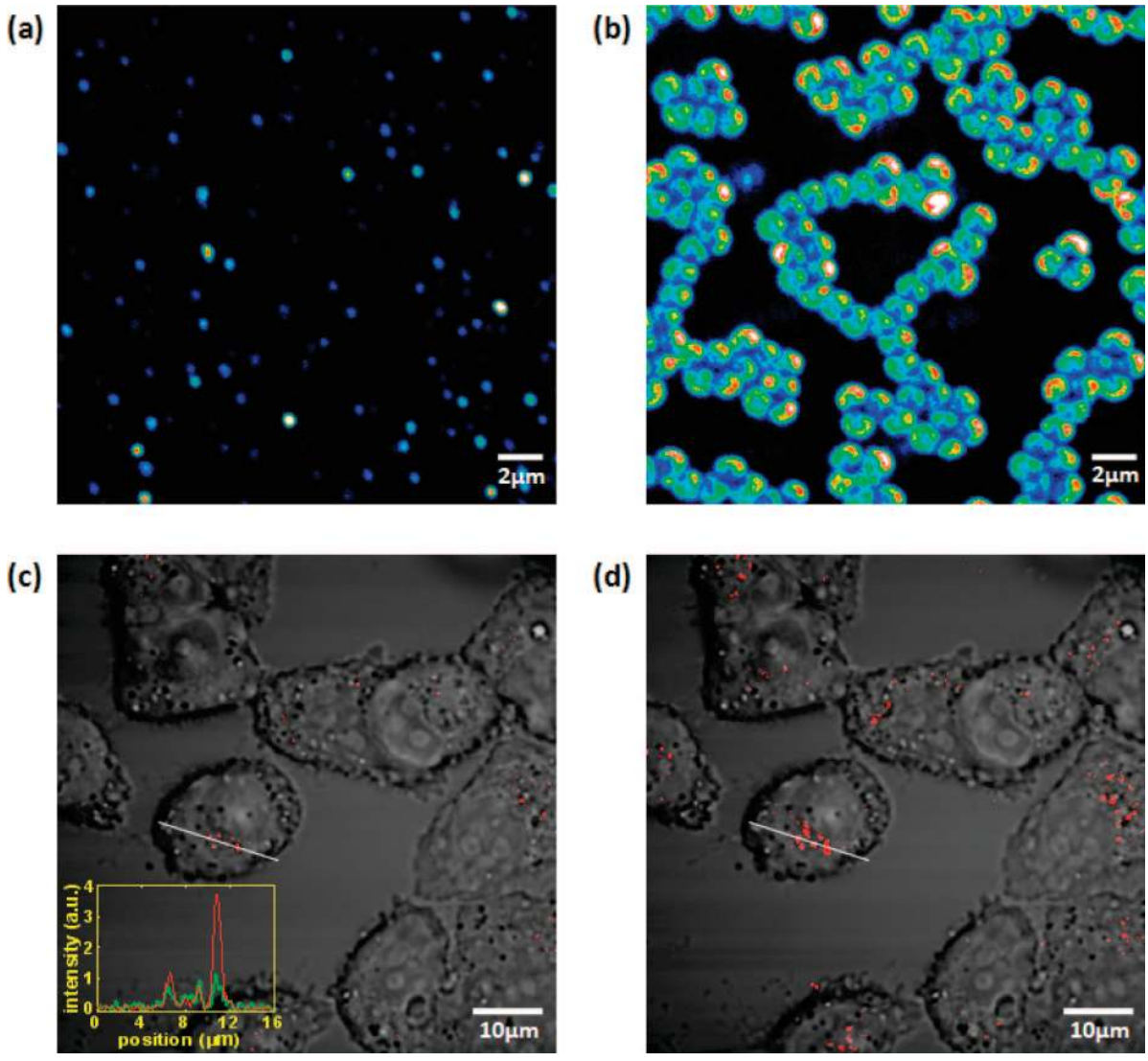

Figure 6. Application of FWM from NR in live cell imaging. (a) FWM image of NRs with 0.4 mW pump beam and 1.3 mW Stokes beam. (b) CARS image of 1-μm melamine beads with 2.5 mW pump and 1.3 mW Stokes beam. The pump power was adjusted to ensure the CARS and FWM intensities were at the same level. (c) Epi-detected image of nanorods (red) overlapped with the transmission image of cells (gray) with the pump and Stokes beams desynchronized. (d) Epi-detected image of nanorods (red) overlapped with the transmission image of cells (gray) with the pump and Stokes beams synchronized. Embedded in (c) are the intensity profiles along the white lines. The green and red curves represent the intensities with the pump and Stokes beams desynchronized and synchronized, respectively.

according to the synchronization of the two beams. We observed an increase of intensity, which is caused by the TPL at the wavelength from 628∼672 nm, when the pump and Stokes beams were synchronized. However, the emission spectra indicate no FWM signal as shown in Figure 5, panels e and f. Although the enhanced TPL can be readily explained as a result of sum frequency excitation, the strong dependence of FWM on the pulse width is striking. We attribute this dependence to the ultrafast electron dynamics in NRs. Because the plasma dephasing time is on the femtosecond time scale,[30] a much stronger plasmon field can be produced with femtosecond pulses than with picosecond pulses at the same energy of approximately picojules, resulting a distinctive FWM peak over the broad TPL background. Previously, nanosecond pulses with microjule pulse energies were needed to generate FWM signal from gold or silver colloids.[31]

For NRs to be used as a NLO imaging agent, we need to make sure that the FWM signal from the NRs is much larger than the background FWM from biological structures. For this purpose, we compared the FWM signal from NR788 with nonresonant CARS from melamine beads using femtosecond pulses at 790 and 1018 nm. Here the melamine beads were used to mimic solid structures in a biological tissue. The Stokes beam power was fixed at 1.3 mW at the sample and the pump beam power was varied until the FWM and CARS signals reached the same level. We chose the brightest NRs for the signal comparison. Even though the overall intensities in Figure 6a appear lower than in Figure 6b, the brightest spots in Figure 6a, which are observable when the NRs have the same orientation as the incident beam polarization, showed similar peak intensities to the CARS signal of the melamine beads. Figure 6a shows the FWM image with a pump power of 0.4 mW. Figure 6b shows the CARS image of 1-μm melamine beads with a pump power of 2.5 mW. Because both FWM and CARS intensities are proportional to the square of the pump power, the FWM intensity from NRs is $(2.5/0.4)^2 \approx 39$ times stronger than the CARS from 1-μm beads. Using the same method, we found the FWM intensity to be 2000 times stronger than the resonant CARS signal from intracellular lipid bodies. Therefore, FWM from NR can be produced at a low excitation

power whereas CARS from polymer or biological material is negligible, making NRs a valid NLO imaging probe.

The application of FWM from NR in live cell imaging is demonstrated in Figure 6, panels c and d. We replaced CTAB on the NR surface by cysteine-octaarginine peptide (GenScript, Piacataway, NJ) to reduce cytotoxicity from CTAB and facilitate cellular uptake.[32] KB cells were incubated with the peptide-conjugated NRs for 8 h prior to imaging. Figure 6c shows the overlay of TPL (red) from NRs and the transmission image of cells (gray). TPL was acquired with desynchronized pump and Stokes beams. Figure 6d shows images from the same cells but with synchronized pump and Stokes beams. We observed more and brighter spots in Figure 6d than in Figure 6c. The inset in the Figure 6c shows the intensity profiles of NRs when the two beams are desynchronized (green) and synchronized (red). These results indicate the potential of using FWM to visualize NRs in a biological system.

In conclusion, we have demonstrated an enhanced FWM signal from NRs under a nonlinear optical microscope. The FWM signal is enhanced not only by surface plasmon resonance but also by aggregation of nanorods. With the pulse energy less than 21 pJ, the FWM can be effectively generated with femtosecond pulses without melting nanorods but not with picosecond pulses. The FWM enables selective imaging of nanorods in live cells. The strong dependence of FWM on nanorod aggregation opens up the opportunity of using NLO signals for aggregation-based chemical sensing.

Acknowledgment. This work was support by NSF Grant CBET 0828832. The authors acknowledge Dr. Jihoon Jeon for the AFM measurement.

Note Added after ASAP Publication. This article was published ASAP on January 21, 2009. References 6, 7, and 9 have been changed. The correct version was published on January 26, 2009.

References and Notes

(1) Sönnichsen, C.; Franzl, T.; Wilk, T.; von Plessen, G.; Feldmann, J.; Wilson, O.; Mulvaney, P. Drastic reduction of plasmon damping in gold nanorods. *Phys. Rev. Lett.* **2002**, *88*, 077402.

(2) Murphy, C. J.; Gole, A. M.; Stone, J. W.; Sisco, P. N.; Alkilany, A. M.; Goldsmith, E. C.; Baxter, S. C., Gold nanoparticles in biology: beyond toxicity to cellular imaging. *Acc. Chem. Res.* **2008**, *41* (12), 1721−1730.

(3) Sun, T.; Diebold, G. J. Generation of ultrasonic waves from a layered photoacoustic source. *Nature* **1992**, *355*, 806–808.

(4) Wang, X.; Pang, Y.; Ku, G.; Xie, X.; Stoica, G.; Wang, L. V. Noninvasive laser-induced photoacoustic tomography for structural and functional in vivo imaging of the brain. *Nat. Biotechnol.* **2003**, *21* (7), 803–806.

(5) Ku, G.; Wang, L. V. Deeply penetrating photoacoustic tomography in biological tissues enhanced with an optical contrast agent. *Opt. Lett.* **2005**, *30*, 507–509.

(6) Farrer, R.; Butterfield, F.; Chen, V.; Fourkas, J. Highly efficient multiphoton-absorption-induced luminescence from gold nanoparticles. *Nano Lett.* **2005**, *5* (6), 1139–1142.

(7) Qu, X.; Wang, J.; Zhang, Z.; Koop, N.; Rahmanzadeh, R.; Huttmann, G. Imaging of cancer cells by multiphoton microscopy using gold nanoparticles and fluorescent dyes. *J. Biomed Opt.* **2008**, *13* (3), 031217.

(8) Wang, H.; Huff, T. B.; Zweifel, D. A.; He, W.; Low, P. S.; Wei, A.; Cheng, J.-X. In vitro and in vivo two-photon luminescence imaging of single gold nanorods. *Proc. Natl. Acad. Sci. USA* **2005**, *102*, 15752–15756.

(9) Park, J.; Estrada, A.; Sharp, K.; Sang, K.; Schwartz, J.; Smith, D.; Coleman, C.; Payne, J.; Korgel, B.; Dunn, A. Two-photon-induced photoluminescence imaging of tumors using near-infrared excited gold nanoshells. *Optics Express* **2008**, *16* (3), 1590–1599.

(10) Kim, H.; Taggart, D. K.; Xiang, C.; Penner, R. M.; Potma, E. O. Spatial Control of Coherent Anti-Stokes Emission with Height-Modulated Gold Zig-Zag Nanowires. *Nano Lett.* **2008**, *8*, 2373–2377.

(11) Kim, H.; Xiang, C.; Güell, A. G.; Penner, R. M.; Potma, E. O. Tunable Two-Photon Excited Luminescence in Single Gold Nanowires Fabricated by Lithographically Patterned Nanowire Electrodeposition. *J. Phys. Chem. C* **2008**, *112* (33), 12721–12727.

(12) Danckwerts, M.; Novotny, L. Optical frequency mixing at coupled gold nanoparticles. *Phys. Rev. Lett.* **2007**, *98*, 026104.

(13) Lippitz, M.; van Dijk, M. A.; Orrit, M. Third-Harmonic generation from single gold nanoparticles. *Nano Lett.* **2005**, *5*, 799–802.

(14) Yelin, D.; Oron, D.; Thiberge, S.; Moses, E.; Silberberg, Y. Multiphoton plasmon-resonance microscopy. *Opt. Express* **2003**, *11* (12), 1385–1391.

(15) Link, S.; El-Sayed, M. A. Spectral properties and relaxation dynamics of surface plasmon electronic oscillations in gold and silver nanodots and nanorods. *J. Phys. Chem. B* **1999**, *103*, 8410–8426.

(16) Murphy, C. J.; Gole, A. M.; Hunyadi, S. E.; Stone, J. W.; Sisco, P. N.; Alkilany, A.; Kinard, B. E.; Hankins, P. Chemical sensing and imaging with metallic nanorods. *Chem. Commun.* **2008**, 544–557.

(17) Tong, L.; Wei, Q.; Wei, A.; Cheng, J. X., Gold nanorods as contrast agents for biological imaging: optical properties, surface conjugation, and photothermal effects. *Photochem. Phtotobiol.* . in press.

(18) Boyd, R. W. *Nonlinear Optics*, 2nd ed.; Academic Press: Boston, 2003.

(19) Vogel, E. M.; Weber, M. J.; Krol, D. M. Nonlinear optical phenomena in glass. *Phys. Chem. Glasses* **1991**, *32*, 231–253.

(20) Chen, C. K.; Heinz, T. F.; Richard, D.; Shen, Y. R. Surface-enhanced second-harmonic generation and Raman scattering. *Phys. Rev. B* **1983**, *27*, 1965–1979.

(21) Boyd, G. T.; Rasing, T.; Leite, J. R. R.; Shen, Y. R. Local-field enhancement on rough surfaces of metals, semimetals, and semiconductors with the use of optical second-harmonic generation. *Phys. Rev. B* **1984**, *30*, 519–526.

(22) Stratton, J. A., *Electromagnetic Theory*; McGraw-Hill Book Company, Inc.: New York, 1941.

(23) Yu, C.; Irudayaraj, J. Quantitative Evaluation of Sensitivity and Selectivity of Multiplex NanoSPR Biosensor Assays. *Biophys. J.* **2007**, *93* (10), 3684–3692.

(24) Chen, H.; Wang, H.; Jung, Y.; Shi, Y.; Zhu, J.; Buhman, K.; Cheng, J.-X., A Multimodal Platform for Nonlinear Optical Microscopy and Microspectroscopy. *Opt. Express*. in press.

(25) Nikoobakht, B.; El-Sayed, M. A. Preparation and growth mechanism of gold nanorods (NRs) using seed-mediated growth method. *Chem. Mater.* **2003**, *15*, 1957–1962.

(26) Calculation of the pulse energy: 1.3 mW from the Stokes laser and 0.4 mW from the pump laser were used for the generation of FWM from gold nanorods. Because the repetition rate is 80 MHz, if the laser power is 1.7 mW, the pulse energy is 1.7 mW/(80×10^6 s^{-1}) = 21 pJ. We started to observe melting of NRs by increasing the pump laser power to 0.8 mW. No melting was observed by increasing the Stokes laser power. Therefore, the power we used for imaging is 50% below the damage threshold.

(27) Shalaev, V. M., *Nonlinear optics of random media: fractal composites and metal-dielectric films*, 1st ed.; Springer: New York, 2000.

(28) Cheng, J. X.; Xie, X. S. Coherent anti-Stokes Raman scattering microscopy: instrumentation, theory, and applications. *J. Phys. Chem. B* **2004**, *108* (3), 827–840.

(29) Wang, H.-W.; Le, T. T.; Cheng, J.-X. Label-free imaging of arterial cells and extracellular matrix using a multimodal CARS microscope. *Opt. Commun.* **2008**, *281* (7), 1813–1822.

(30) Park, S.; Pelton, M.; Liu, M.; Guyot-Sionnest, P.; Scherer, N. F. Ultrafast Resonant Dynamics of Surface Plasmons in Gold Nanorods. *J. Phys. Chem. C* **2007**, *111*, 116–123.

(31) Safonov, V. P.; Danilova, Y. E.; Drachev, V. P.; Perminov, S. V. Optical Nonlinearities in Metal Colloidal Solutions. In *Optics of Nanostructured Materials*, 1st ed.; Markel, V. A., George, T. F., Eds.; Wiley-Interscience: New York, 2001.

(32) Khalil, I. A.; Kogure, K.; Futaki, S.; Harashima, H. High Density of Octaarginine Stimulates Macropinocytosis Leading to Efficient Intracellular Trafficking for Gene Expression. *J. Biol. Chem.* **2006**, *281* (6), 3544–3551.

JP810852C